Geophysical Research Letters

RESEARCH LETTER
10.1029/2019GL082411

Seismic Noise Interferometry Reveals Transverse Drainage Configuration Beneath the Surging Bering Glacier

Zhongwen Zhan[1]

[1]Seismological Laboratory, California Institute of Technology, Pasadena, CA, USA

Key Points:
- Noise interferometry across Bering Glacier reveal 1-2% seismic velocity reduction during its latest surge
- The changes require anisotropic weakening of the glacial base with elongated water pockets transverse to ice flow
- We interpret the results as evidences for distributed subglacial water flow through a network of basal crevasses

Supporting Information:
- Supporting Information S1

Correspondence to:
Z. Zhan,
zwzhan@caltech.edu

Citation:
Zhan, Z. (2019). Seismic noise interferometry reveals transverse drainage configuration beneath the surging Bering Glacier. *Geophysical Research Letters*, *46*, 4747–4756. https://doi.org/10.1029/2019GL082411

Received 8 FEB 2019
Accepted 18 APR 2019
Accepted article online 25 APR 2019
Published online 3 MAY 2019

Abstract Subglacial drainage systems are known to critically control ice flows, but their spatial configuration and temporal evolution are poorly constrained due to inaccessibility. Here we report a 12-year-long monitoring of the drainage underneath Bering Glacier, Alaska, by correlating ambient noise recorded at two seismic stations on the sides of the glacier. We find that the seismic surface waves traveling across Bering Glacier slowed down by 1–2% during its latest 2008–2011 surge, likely due to the switch of the subglacial drainage from a channelized system to a distributed system. In contrast to current models, the relative amplitude of velocity reductions for Rayleigh and Love waves requires the distributed drainage to be highly anisotropic and aligned perpendicular to the ice flow direction. We infer that the subglacial water flow is mainly through a network of transverse basal crevasses during surges and thus can sustain the high water pressure and ice flow speed.

Plain Language Summary Water underneath glaciers strongly controls how ice flows. However, it is difficult to map how water flows under the cover of hundreds or thousands of meters of ice. Here we propose a new approach to image and monitor water in glaciers, by using seismic waves continuously excited by the ocean and atmosphere. With sensors on both sides, we can measure the time seismic waves take to travel across a glacier. More water in glacier can slow down the seismic waves. For Bering Glacier, Alaska, we detected a substantial slowdown of seismic waves from 2008 to 2010, which coincides with a period when the ice flow accelerated by a factor of 10. We interpret the observed seismic slowdown as caused by water flowing through a network of crevasses near the base of the glacier.

1. Introduction

Fast-flowing glaciers contribute disproportionately to the global ice losses and sea level rise (Clarke, 1987). However, the mechanics behind fast ice flow and how they respond to external forcing (e.g., increased surface melt and tides) are still unclear (Schoof & Hewitt, 2013). Surge-type glaciers (semi)periodically switch between slow and fast flows under internal instability and hence provide a unique window to the mechanisms and stability of ice flows (Meier & Post, 1969; Raymond, 1987). Numerous field observations and theoretical analyses suggest that subglacial drainage systems play a critical role in surges (Björnsson, 1998; Björnsson et al., 2003; Eisen et al., 2005; Flowers, 2015; Harrison et al., 1994; Kamb, 1987; Kamb et al., 1985). During surges, the drainage switches from a channelized, low-pressure system to a distributed, high-pressure system, which partially decouples the glacier from the base and promotes fast basal sliding (Flowers, 2015; Kamb, 1987; Kingslake & Ng, 2013; Schoof, 2010).

However, the spatial configuration of the distributed drainage system is inaccessible to most field methods, especially during surges when access to the surface may become difficult. It can only be inferred from localized hydrological observations (e.g.,Bartholomaus et al., 2008 ; Björnsson, 1998 ; Kamb et al., 1985), largely unconstrained geophysical modeling (e.g.,Kingslake & Ng, 2013 ; Schoof, 2010), and more recently remote observations of flow-induced seismic noise (Gimbert et al., 2016). Based on the extensive field observations made for the 1982–1983 surge of Variegated Glacier, Kamb et al. (1985) proposed the linked-cavities model, in which the drainage system is described as a network of water-filled cavities formed behind bed protuberances (Lliboutry, 1968). Narrow passageways connect the cavities and throttle the water flow. The cavity network is kept stable by a balance between glacial sliding and ice creep closure but can switch to a channelized system and shut down the surge via depressurization if the water flux is above a certain threshold (Kamb, 1987). The linked-cavities model can explain many observations of surges (e.g., high water pressure, slow

water out flux, and flood after surge; Björnsson, 1998) but assumes impermeable glacial beds. This assumption is challenged by observations that many glaciers, including surge-type glaciers, are underlain by a soft and potentially permeable till layer that appears to accommodate a large fraction of the basal motion (Blankenship et al., 1987; Engelhardt et al., 1990; Harrison & Post, 2003), and possibly for Bering Glacier in particular (Fleisher et al., 2006). Therefore, alternative soft-bed drainage configurations during rapid sliding were proposed (Flowers, 2015), such as a laminar water flow of variable thicknesses (Weertman, 1972), porous flow through till (Fowler et al., 2001) and canals cutting into the till layer (Ng, 2000; Walder & Fowler, 1994). These soft-bed configurations can also sustain high water pressure over distributed areas to weaken the till layer and reduce basal resistance to ice flow. Current field observations do not seem able to distinguish the hard-bed and soft-bed configurations or whether there exists a single mechanism for surges (Harrison & Post, 2003; Murray et al., 2003; Pritchard, 2005; Sevestre et al., 2015).

In this paper, we use seismic surface waves that travel laterally across a surging glacier to interrogate the subglacial drainage system. As the drainage switches from a low-pressure channelized system to a high-pressure distributed system, the reduced mechanical coupling between ice and glacial bed affects not only ice flow but also the overall elastic properties of the ice-water-till-bedrock system. Widespread water pockets at the glacier base can slow down seismic waves as a bulk equivalent low-velocity layer near the ice/bed interface. Here we report a full cycle of seismic monitoring across Bering Glacier, Alaska, before, during, and after its 2008–2011 surge to interrogate spatial configuration and temporal evolution of basal drainages.

2. Data and Results

Bering Glacier is the largest and longest glacier on the North America continent (Figure 1a). It surged every 15–20 years in the last century with each episode lasting about 2 years (Burgess et al., 2012; Molnia & Post, 2010; Turrin et al., 2013). The latest surge started in summer 2008 and consisted of two stages (Burgess et al., 2012). The first stage lasted over 10 months, during which the ice mostly moved from the up-glacier reservoir zone to the midglacier section (Figure 1b). The ice flow accelerated from the quiescence speed of 0.5 m/day to a maximum speed of 7 m/day in this stage. The second stage started sometime during 2010 and reached a peak flow speed of 9 m/day in 2011. The ice moved from the midglacier section further down-glacier (Figure 1b) and advanced the terminus by 2–4 km (Turrin et al., 2013). Repeated airborne radar survey of the ice elevation show changes of up to 100 m but on average of about 20 m where our seismic observations sample the glacier (Burgess et al., 2012).

2.1. Twelve-Year Seismic Noise Correlation Across the Bering Glacier

In 2005, two broadband seismic stations, GRIN and KHIT, were deployed on the sides of Bering Glacier (Figure 1a), as part of the SainT Elias Erosion/tectonics Project (Worthington et al., 2012), and later became part of the Alaska Regional Seismic Network. The path connecting GRIN and KHIT crosses the midglacier section of Bering Glacier at a high angle (~60°, Figure 1a). The 12-year-long (2005–2017) continuous records of ambient seismic noise allow us to monitor the glacier structure between the two stations, before, during, and after the 2008–2011 surge. Repeated estimations of the impulse responses between two stations obtained by correlating their seismic noise recordings can reveal subtle structural changes, including seismic velocity changes as small as 0.1%, due to earthquakes (Brenguier et al., 2008), volcanic eruptions (Duputel et al., 2009), drought (Clements & Denolle, 2018), and ice melting (Walter et al., 2015; Mordret et al., 2016; Toyokuni et al., 2018).

We cross correlated the three-component records of seismic noise at GRIN and KHIT in 30-min segments and then stacked the correlation functions in 60-day moving windows and 15-day overlaps. Because the GRIN-KHIT pair is oriented in the north-south direction (azimuth~12° east of north), the east-east and vertical-vertical correlations approximate the Love and Rayleigh Green's functions between the stations, respectively. The overlapping bimonthly correlation functions show high coherency throughout the 12 years (see supporting information Figure S1 for Love and Rayleigh correlations in the frequency band of 0.5–1 Hz). This allows us to accurately measure time shifts of windowed waveforms on individual correlations relative to the reference correlation function, derived by stacking all the correlation functions. As shown in Figure 2a for the 0.5–1 Hz Love waves, time shifts in the time window of [5 s, 25 s], corresponding to the direct waves (arriving at about 8 s) and early coda waves propagating from GRIN to KHIT, switch from positive to negative in 2008 and to positive again in 2013/2014. This suggests that the Love wave speed was slower between

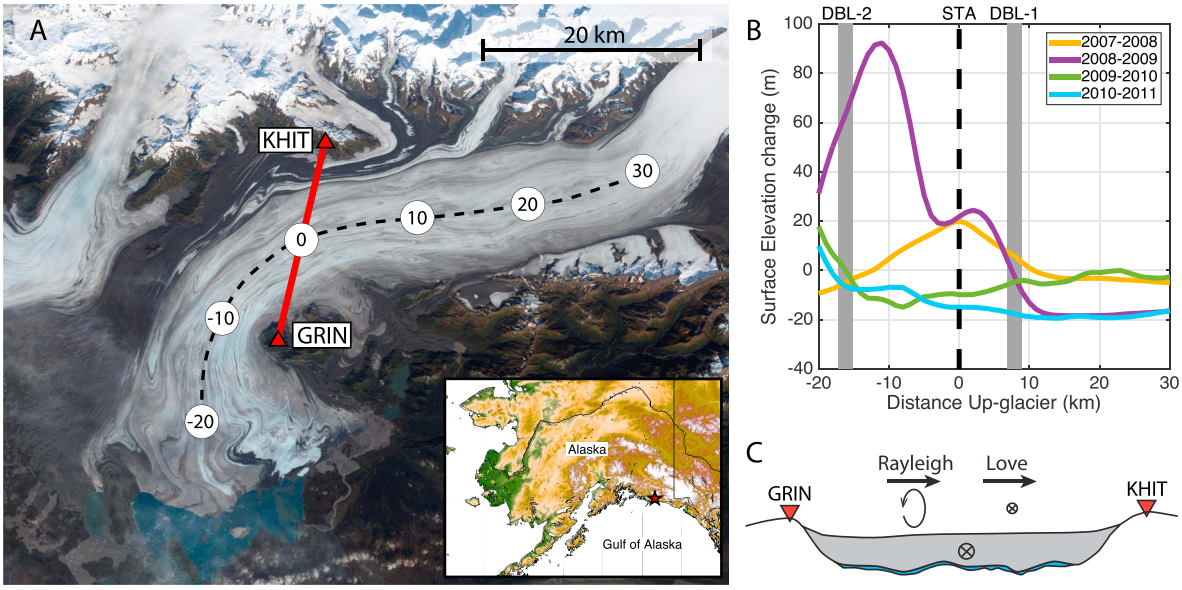

Figure 1. Bering Glacier and its 2008–2011 surge. (a) Landsat image of Bering Glacier and locations of the GRIN and KHIT seismic stations. The station pair crosses the glacier central middle line (dashed line) at a high angle. Dots with numbers mark the up-glacier distances from the crossing point in kilometers. Red star in the inset indicates the location of Bering Glacier. (b) Yearly surface elevation changes during the 2008–2011 surge along the glacier (Burgess et al., 2012). The distance up-glacier is along the dashed line in (a). DBL-1 and DBL-2 are dynamic balance lines (DBL) for the two stages of surge (Burgess et al., 2012), separating the reservoir zones and receiving zones. Black dashed line "STA" marks the sampling point between GRIN and KHIT. (c) Illustrated cross section view from east along the two stations, in which the ice flows away from readers. For Rayleigh and Love waves propagating from GRIN to KHIT, their particle motions are perpendicular and parallel to ice flow direction, respectively.

2008 and 2013 than the 12-year average. In the time window [−25 s, −5 s], which corresponds to the waves propagating from KHIT to GRIN, the patterns of time shifts are similar to the positive side but of opposite polarity. This odd symmetry of time shifts is a strong sign for real structural changes between stations and difficult to explain by changes of noise sources (Brenguier et al., 2008; Zhan et al., 2013). Later coda waves ($t < -25$ s or $t > 25$ s) do not show larger time shifts, suggesting that the structural changes are focused around the station pair's path across the glacier, instead of being distributed in a broad area (Obermann et al., 2013).

Figure 2b displays the time series of bimonthly velocity reductions for the 0.5–1 Hz Love and Rayleigh waves based on the time shifts measured in the [−25 s, −5 s] and [5 s, 25 s] windows, referenced to the average between 2005 and 2007. For the Love waves (blue curve in Figure 2b), we observe a clear slowdown starting from 2008, peaking at almost 2% in 2011, and then a slow recovery from 2012 to 2016. By the end of 2016 the Love wave speed returned to the same level as before the surge. The start and peak of the velocity reduction coincide with the start and peak of the glacier surge (Burgess et al., 2012). There is also a seasonal pattern on top of the long-term variation, with slowdown in early summer followed by recovery in falls and winters. The Rayleigh wave speed shows a similar trend, although the amplitude is about half of that of the Love waves, likely due to their different polarities of particle motion with respect to the ice flow direction (Figure 1c). A control station pair (BARK-ISLE, Figure S2) with a similar orientation but sampling areas not affected by the Bering Glacier surge shows neither long-term nor seasonal variations, with 0.1% of random fluctuations (green curve in Figure 2b). This further confirms that the observed temporal variations in Rayleigh and Love speeds between GRIN and KHIT are caused by physical changes in the glacier during surge, not by coincidental changes of noise source distribution or a change in the crust over a broad area.

2.2. Depth of Change Based on Frequency-Dependent Sensitivity of Surface Waves

Glacier thickness, morphology, and hydrology all change significantly during surges. Extensive surface crevasses developed during surge could slow down the top ice layer down to tens of meters (Herzfeld et al., 2013; Kamb et al., 1985). The entire ice column's seismic speed may be lowered by higher water content under nearby hydrostatic water pressure (Kamb et al., 1985). The ice thickness also varied by about 20 m in the

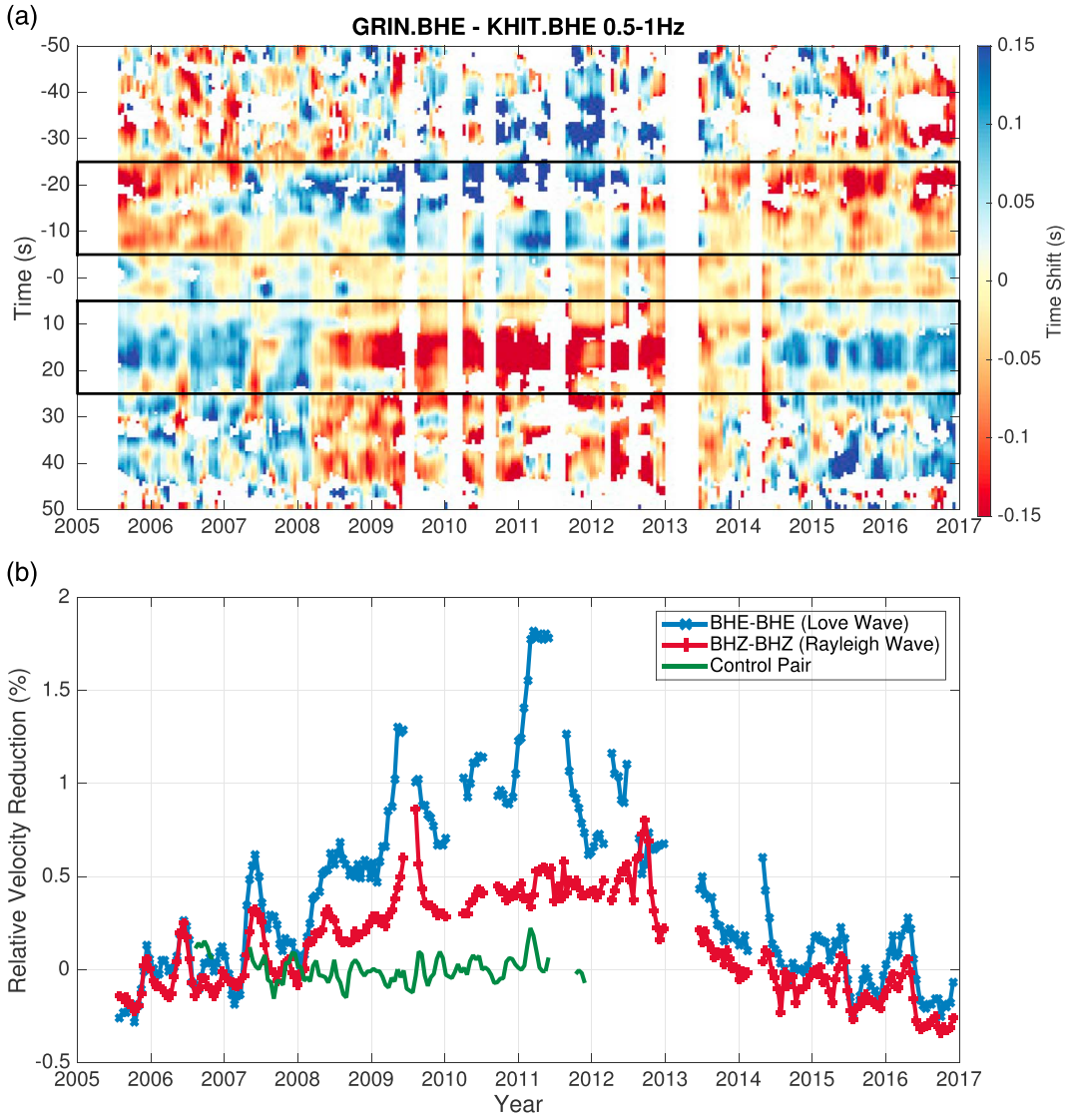

Figure 2. Noise monitoring across Bering Glacier. (a) Time shifts of windowed waveforms on bimonthly correlations relative to the reference correlation, for the east-east (Love) component and the 0.5–1 Hz frequency band. Blank patches are due to missing data or noisy correlations. Note that the measurements on the acausal side (negative time, waves propagating from KHIT to GRIN) are generally noisier than those on the positive side, likely due to seismic noise originating mostly from the ocean to the south, propagating from GRIN to KHIT. Black rectangles highlight the (5 s, 25 s) and (−25 s, −5 s) windows used in relative velocity change calculations. (b) Time series of relative velocity reductions for GRIN-KHIT east-east and vertical-vertical components in the 0.5–1 Hz frequency band. Gaps are due to missing data or noisy correlations. The green curve is for vertical-vertical correlations on a nearby station pair, BARK-ISLE (Figure S2), sampling outside the active surge section of Bering Glacier, as a control pair.

section of Bering Glacier sampled by the GRIN-KHIT pair (Burgess et al., 2012). We will need to disentangle contributions of all these factors before attributing all or part of the observed seismic wave speed changes to the basal drainage system.

We synthetically evaluate the impact of four end-member scenarios to Rayleigh and Love wave speeds as a function of frequency (i.e., dispersion): slowed firn layer, slowed ice column, thicker ice, and decreased basal coupling by a slower till layer. We combine results from previous surveys in the Bering Glacier area and other glaciers to build a starting 1-D model (Figure 3a; see supporting information for details). An important feature of this 1-D model is that the shear wave speed (V_S) of the ice layer and the top sediment layer are similar, with a low-velocity till layer sandwiched in between (Blankenship et al., 1987; Fleisher et al.,

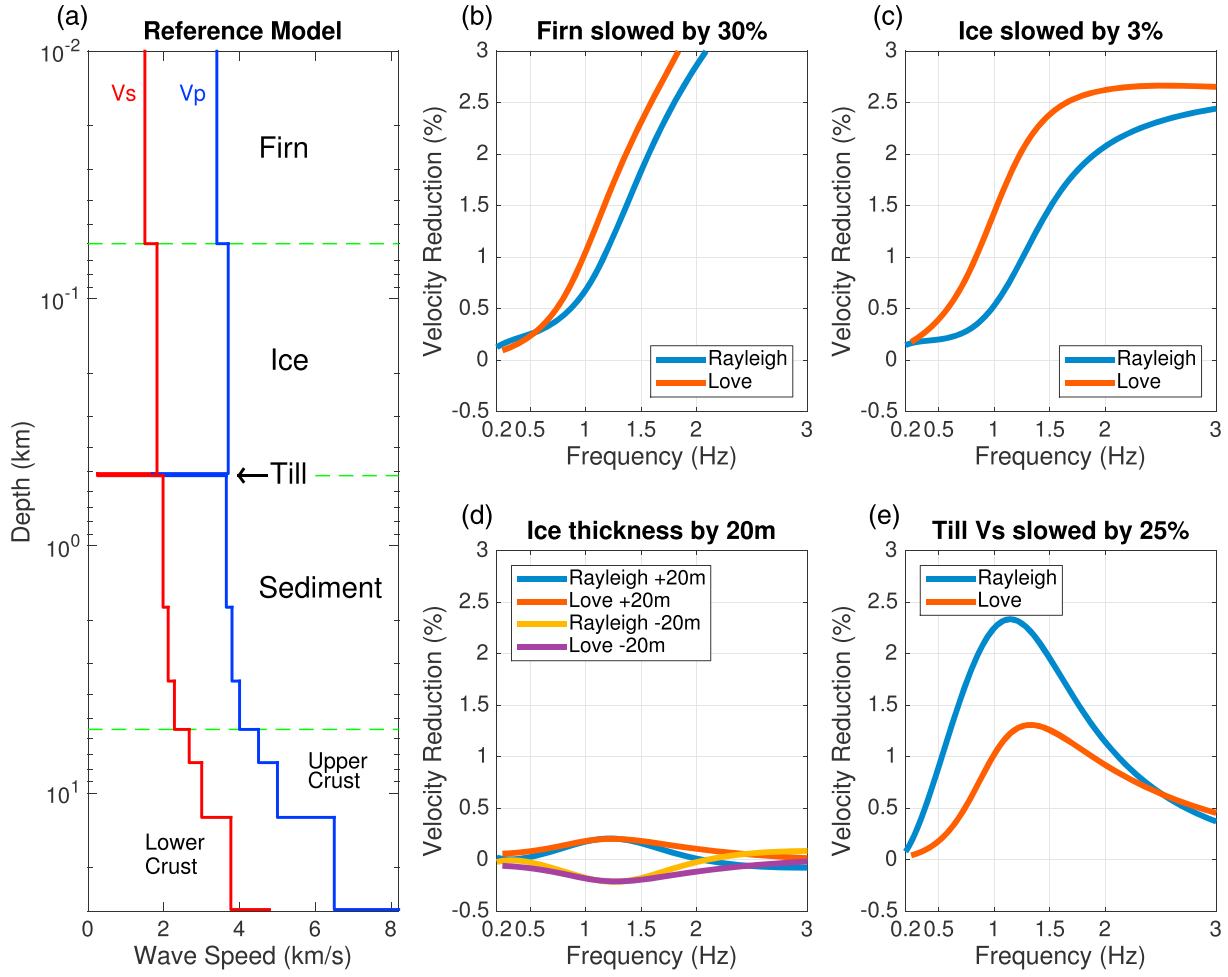

Figure 3. Predictions of frequency-dependent velocity reductions from four end-member scenarios. (a) Reference 1-D model that represents the glacier before surge consists of firn, ice, till, and rock layers. We calculate the change of Rayleigh and Love wave phase velocities as a function of frequency for (b) 30% slower firn layer, (c) 3% slower ice column, (d) 20-m changes in ice thickness, and (e) 25% slower till V_S, respectively. In (d), the ice thickness can be either 20 m thicker or 20 m thinner as observed around the station pair during the two stages of the surge (Figure 1b).

2006; Worthington et al., 2012). We then perturb the 1-D model and numerically calculate velocity reduction in the frequency band of 0.2–3 Hz with a propagation matrix method. The four end-member scenarios predict significantly different dispersions to Rayleigh and Love wave speeds. Intense surface crevassing or a bulk slower ice column would produce the strongest changes at high frequencies (>1.5 Hz), while a weaker basal layer would predict a reduction of surface wave speed peaked at frequencies near 1 Hz. Changes in ice thickness have negligible impact on surface wave speed due to the similar shear wave velocity in the ice and sedimentary rock layers below Bering Glacier. Therefore, resolving the frequency dependence of velocity change between GRIN and KHIT will help determine the depth range and physical cause of the observed changes.

To resolve the frequency dependence of velocity changes, we repeat the measurements for 0.5–1 Hz (Figure 2b) in many overlapping frequency bands between 0.2 and 2 Hz for which the noise correlation functions show high coherency and signal-to-noise ratios. We then assume the measured velocity change for a particular band is an arithmetic mean of the frequency-dependent changes within the band, so that we can linearly invert the changes measured in all the bands for a continuous frequency-dependent velocity change between 0.2 and 2 Hz, as shown in Figure 4. We apply regularization with a Gaussian model covariance matrix with a 10-day correlation length in time and a 0.2-Hz correlation length in frequency. The resulting velocity variation estimates are concentrated between 0.4 and 1.5 Hz, with the maximum reductions (~2% for Love waves) around 0.8–1.2 Hz (Figure 4c), which is only consistent with the scenario of a

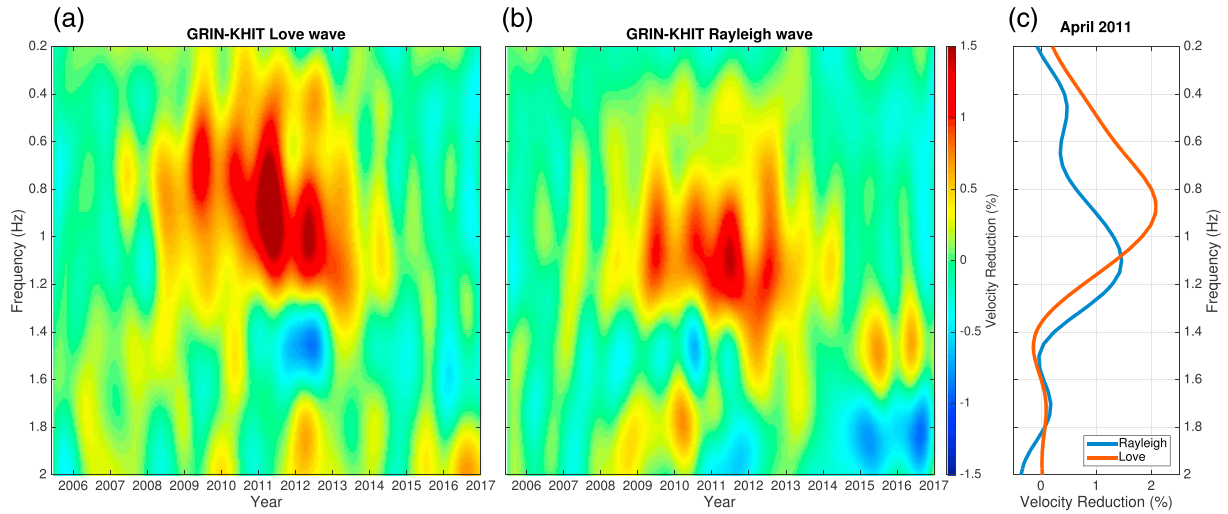

Figure 4. Observed frequency dependences of velocity reductions, for (a) Love wave and (b) Rayleigh wave, referenced to the average between 2005 and 2007. The strong reductions (red colors) are concentrated between 0.4 and 1.5 Hz. On top of the long-term changes related to the surge, seasonal patterns show velocity reductions in early summers and recoveries in falls and winters. (c) Velocity reductions in April 2011, when surge reached peak flow speed (Burgess et al., 2012), show maximum reductions between 0.8 and 1.2 Hz, up to 1.5% for Rayleigh waves and 2% for Love waves.

weakened basal layer in Figure 3. This suggests that the physical cause of the observed seismic velocity change is dominated by processes near the base of Bering Glacier, instead of near surface or throughout the ice column.

2.3. Evidence for Anisotropic Change in the Basal Layer

Our observations also suggest that the change in the basal layer is anisotropic. The observed velocity changes in individual frequency bands (e.g., 0.5–1 Hz in Figure 2b) and after inversion (Figure 4) show larger reduction in Love wave speed than in Rayleigh wave speed. Quantitatively, the peak Rayleigh velocity reduction (δC_R) in 2011 is about 75% of the peak Love velocity reduction (δC_L). This difference is opposite from the prediction based on an isotropically weakened basal layer (Figure 3e), where δC_R is about twice of δC_L. We hypothesize that the spatial configuration of the distributed subglacial drainage network causes a bulk anisotropic seismic velocity reduction for seismic surface waves with about 1- to 4-km wavelengths. Because the GRIN-KHIT pair is at a high angle to the ice flow direction, the Rayleigh and Love wave particle motions are approximately perpendicular and parallel to the ice flow, respectively (Figure 1c). When propagation direction is the same, seismic waves with particle motion aligned with the long axes of small-scale heterogeneities is less affected than waves with particle motion perpendicular to the long axis (e.g., Crampin, 1985 ; Savage, 1999). In the scenario of drainage networks, the heterogeneities are water pockets in cavities, pathways, or crevasses. Because water has lower seismic speeds than ice and rock, a glacial base with increasing areal fraction of water will reduce the average seismic velocity as observed. If the water pockets have an anisotropic geometry with the long axes perpendicular to the direction of ice flow and to the Love wave particle motion, then the Love waves will be preferentially slowed down compared to the Rayleigh waves, as observed.

Full 3-D finite-difference simulations of wave propagation confirm such an anisotropic effect. We take the ice-till-rock model in Figure 3a as the reference, then replace a certain fraction of the till elements with water ($V_P = 1{,}500$ m/s, $V_S = 0$ m/s; Figure 5a). The water pockets, 10 m wide and 10–200 m long as constrained by the grid size of the finite-difference simulation, are distributed randomly but aligned along the same direction to mimic the potentially anisotropic subglacial drainage. We then measure the Rayleigh and Love wave speeds in a fan shot with all the receivers at the same 12.5-km distance from the source (Figure 5a). When the aspect ratio of the water pockets is 1:1 (i.e., isotropic), we obtain an azimuth-independent ratio between Rayleigh and Love wave speed reductions ($\delta C_R/\delta C_L$, Figure 5b). As the aspect ratio increases, the Love wave speed reduces more for azimuths aligned with the long axis of water pockets, while the Rayleigh wave speed drops more for the pairs perpendicular to the long axis (Figure 5b). Only a water pocket geometry with aspect ratio close to 1:20 and parallel to the station pair could explain our observation of $\delta C_R/\delta C_L = 0.75$. Therefore, our observation of Rayleigh and Love velocity reductions during the surge require a highly anisotropic

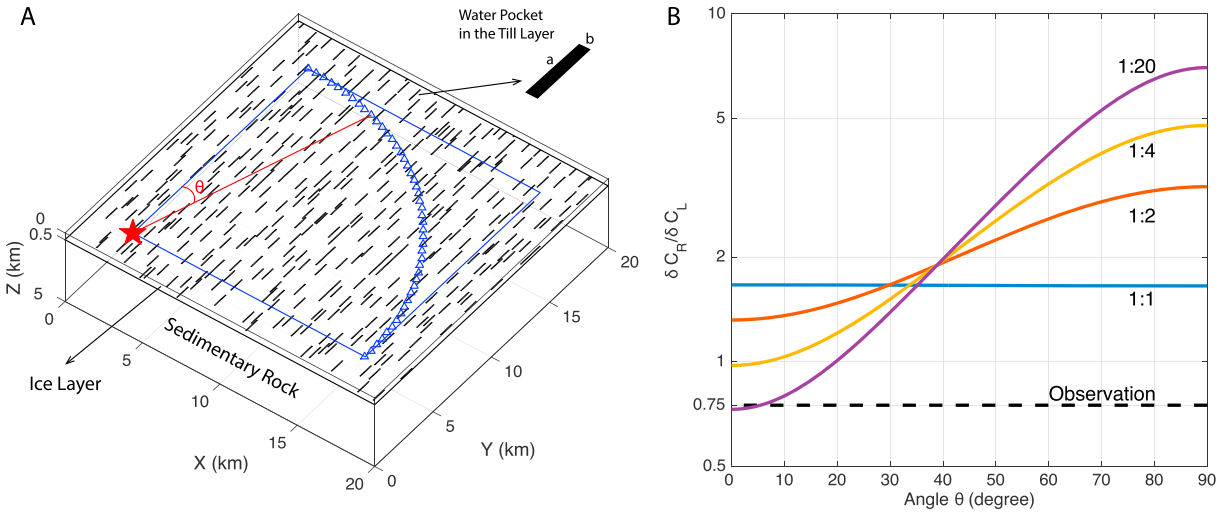

Figure 5. Anisotropic velocity reductions due to elongated water pockets between ice and rock. (a) Setup of 3-D simulations with the 1-D model in Figure 3a as the reference model. Black rectangles at 500-m depth represent randomly distributed water pockets within the till layer aligned in the *Y* axis direction. We simulated Rayleigh and Love waves from the source (red star) to an arc of stations at the same distance (blue triangles) to evaluate velocity reductions due to the inclusion of water pockets, at different angles θ with respect to the long axes of water pockets. (b) Ratios of Rayleigh and Love velocity reductions as a function of angle θ, for water pockets of different aspect ratios. The observed ratio of 0.75 is shown as the horizontal dashed line, requiring water pockets of 1:20 aspect ratio and aligned with the wave propagation direction (i.e., small θ).

drainage system more or less perpendicular to the ice flow (Figure 6a). Finally, to account for the observed 1–2% reduction in the Love wave speed during surge, the water pockets need to cover 10–20% of the total basal area, although this estimate depends on the height and geometry of the water pockets.

2.4. Physical Cause of the Anisotropic Weakening of the Basal Layer

None of the existing models of glacial drainage systems appear to fit the required anisotropy. The soft-bed drainage configurations that involve porous flow or canals would predict long axes following ice flow direction due to the shear deformation of the till layer. Spatial configuration of hard-bed drainage is more controlled by basal topography, which can have long axes aligned or perpendicular to ice flows (e.g., drumlins and moraines). But only basal topographic features underneath fast-flowing glaciers have the high aspect ratio required by our observations, and they are elongated along the ice flow direction, not perpendicular (King et al., 2009). It remains to be explored if specific combinations of basal topography and ice flow speed can produce wave-type cavities with the required orientation and aspect ratio (e.g.,Kamb, 1987 ; Vivian, 1980).

Here we propose that a network of water-filled basal crevasses under high water pressure cause the observed anisotropic weakening near the glacier base. Both surface and basal crevasses develop extensively during glacier surges and usually have high aspect ratios. They align perpendicular to ice flow due to the along-flow extension. Basal crevasses are not observed as easily as the surface crevasses (Harper et al., 2010; Walter et al., 2010) but are known to exist widely in surging glaciers. Actually, crevasse squeeze ridges near glacier terminus are unique indicators of surge-type glaciers (Farnsworth et al., 2016; Lovell et al., 2015; Sharp, 1985). They form when soft sediment is squeezed into the basal crevasses near the end of surges and get preserved after glaciers retreat.

The slow recovery of seismic velocity reduction after surge also supports the basal crevasse explanation. Figure 6b shows the relative velocity change for Love waves at 1 Hz, with two sharp jumps in early summers of 2008 and 2010 at the starts of the two stages. However, the seismic velocity reduction recovers much more slowly over the 5 years from the peak at 2011 to the end of 2016 (Figure 6b). As surge stops, the subglacial drainage system quickly switches back to the more efficient channelized system, and the basal coupling would increase almost instantaneously. Therefore, the slow recovery suggests that the processes causing the seismic velocity reductions can start quickly but need time to recover not only by the change of water distribution which should recover quickly after the postsurge flood (Kamb et al., 1985). On the other hand, a basal crevasse network will not heal quickly, because sediment fills in to keep them open, and water

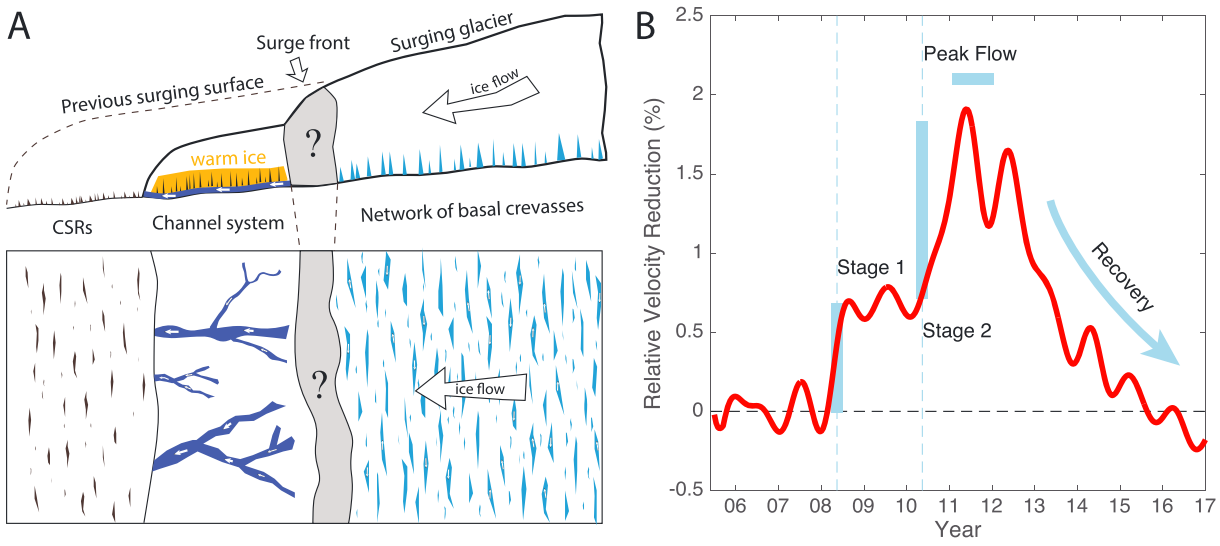

Figure 6. Conceptual interpretation of our noise monitoring results. (a) Basal crevasses generated behind surge front have high aspect ratios and are aligned perpendicular to ice flow, as required by our observations of Rayleigh and Love velocity reduction. A linked network of basal crevasses may serve as pathways of water in the distributed drainage system during surge, after the switch from the channelized drainage system before surge. Therefore, water would flow transversely to ice flows and has inefficient downstream component. After surge stops, sediments and water filling the crevasses would warm the bottom ice layer (Barrett et al., 2008; Murray et al., 2000) and eventually produce crevasse squeeze ridges once the advanced glacier terminus retreats (Lovell et al., 2015; Sharp, 1985). The bimonthly average applied in our seismic observations does not allow us to resolve the process at the surge front on how the switch of drainage system happens. (b) Love wave velocity change at 1 Hz from Figure 4b, showing two sharp reductions in 2008 and 2010 summers, and a slow recovery after the peak over 5 years. The slow recovery may be due to the healing process of the basal crevasses.

circulation will warm up the ice surrounding crevasses as well. Therefore, the seismic velocity will recover slowly over the years, as observed in our data, until the crevasses completely close or the crevasse-filling sediment becomes compact. Murray et al. (2000) reported a "warm ice" layer behind an abandoned surge front using ground penetration radar and seismic images. Later, Barrett et al. (2008) found that the warm-ice layer may consist of sharp lens structures oriented at high angles to the glacier base. We argue that these observations support our basal crevasse explanation.

3. Discussion and Conclusions

In situ observations made by Harper et al. (2010) on Bench Glacier, Alaska, demonstrated that basal crevasses could contribute significantly to water storage capacity and potentially modulate basal water pressure. Here our seismic monitoring of Bering Glacier shows that the basal crevasses are widespread and dominant features during the surge, compared with other proposed configurations (e.g., cavities, canals, and porous flows). The seismic observations are not sensitive to whether the extensive basal crevasses are interconnected, but if the high connectivity observed by Harper et al. (2010) applies, a basal crevasses network linked through crevasse tips and/or basal cavities may serve as a critical component of the subglacial or englacial drainage system during surges. The orientation of the basal crevasses would force water to flow transversely to ice flow, and thus the downstream component of water flow is greatly reduced. This helps sustain the high water pressure and fast ice flows (Kamb et al., 1985). This linked-crevasses hypothesis for glacier surge works for both hard-bed and soft-bed cases and is also consistent with the field observations of crevasse squeeze ridges in front of surge-type glaciers and warm ice behind previous surge front. Finally, the basal crevasses left after surges may provide significant englacial water storage capacity that has been shown to be necessary to explain observed wintertime pressure oscillations and surge initiations (Lingle & Fatland, 2003; Schoof et al., 2014).

Acknowledgments
I am thankful for the Paul Silver enhancement award from IGPP, UC San Diego, which helped start this project, and the Terrestrial Hazard Observation and Reporting (THOR) fund at Caltech for supporting the project. This work benefitted from discussions with Timothy Bartholomaus, Victor Tsai, Rick Aster, and Fabian Walter and comments from Florent Gimbert and an anonymous reviewer. The seismic data used in this study are from the Alaska Regional Network (https://doi.org/10.7914/SN/AK), downloaded through the Incorporated Research Institutions for Seismology (IRIS). I thank Voon-Hui Lai for helping set up the 3-D finite-difference simulations. The satellite image of Bering Glacier in Figure 1a is from the Landsat 7 Science Team.

References

Barrett, B. E., Murray, T., Clark, R., & Matsuoka, K. (2008). Distribution and character of water in a surge-type glacier revealed by multi-frequency and multipolarization ground-penetrating radar. *Journal of Geophysical Research*, *113*, F04011. https://doi.org/10.1029/2007JF000972

Bartholomaus, T. C., Anderson, R. S., & Anderson, S. P. (2008). Response of glacier basal motion to transient water storage. *Nature Geoscience*, *1*(1), 33–37.
Björnsson, H. (1998). Hydrological characteristics of the drainage system beneath a surging glacier. *Nature*, *395*(6704), 771.
Björnsson, H., Pálsson, F., Sigurđsson, O., & Flowers, G. E. (2003). Surges of glaciers in Iceland. *Annals of Glaciology*, *36*, 82–90.
Blankenship, D. D., Bentley, C. R., Rooney, S. T., & Alley, R. B. (1987). Till beneath ice stream B: 1. Properties derived from seismic travel times. *Journal of Geophysical Research*, *92*(B9), 8903.
Brenguier, F., Campillo, M., Hadziioannou, C., Shapiro, N., Nadeau, R. M., & Larose, E. (2008). Postseismic relaxation along the San Andreas fault at Parkfield from continuous seismological observations. *Science*, *321*(5895), 1478–1481.
Burgess, E. W., Forster, R. R., Larsen, C. F., & Braun, M. (2012). Surge dynamics on Bering Glacier, Alaska, in 2008–2011. *The Cryosphere*, *6*(6), 1251–1262.
Clarke, G. K. C. (1987). Fast glacier flow: Ice streams, surging, and tidewater glaciers. *Journal of Geophysical Research*, *92*(B9), 8835.
Clements, T., & Denolle, M. A. (2018). Tracking groundwater levels using the ambient seismic field. *Geophysical Research Letters*, *45*, 6459–6465. https://doi.org/10.1029/2018GL077706
Crampin, S. (1985). Evaluation of anisotropy by shear-wave splitting. *Geophysics*, *50*(1), 142–152.
Duputel, Z., Ferrazzini, V., Brenguier, F., Shapiro, N., Campillo, M., & Nercessian, A. (2009). Real time monitoring of relative velocity changes using ambient seismic noise at the Piton de la Fournaise volcano (La Réunion) from January 2006 to June 2007. *Journal of Volcanology and Geothermal Research*, *184*(1-2), 164–173.
Eisen, O., Harrison, W. D., Raymond, C. F., Echelmeyer, K. A., Bender, G. A., & Gorda, J. L. (2005). Variegated Glacier, Alaska, USA: A century of surges. *Journal of Glaciology*, *51*(174), 399–406.
Engelhardt, H., Humphrey, N., Kamb, B., & Fahnestock, M. (1990). Physical conditions at the base of a fast moving Antarctic ice stream. *Science*, *248*(4951), 57–59.
Farnsworth, W. R., Ingólfsson, Ó., Retelle, M., & Schomacker, A. (2016). Over 400 previously undocumented Svalbard surge-type glaciers identified. *Geomorphology*, *264*, 52–60.
Fleisher, P. J., Lachniet, M. S., Muller, E. H., & Bailey, P. K. (2006). Subglacial deformation of trees within overridden foreland strata, Bering Glacier, Alaska. *Geomorphology*, *75*(1-2), 201–211.
Flowers, G. E. (2015). Modelling water flow under glaciers and ice sheets. *Proceedings: Mathematical, Physical and Engineering Sciences*, *471*(2176).
Fowler, A., Murray, T., & Ng, F. (2001). Thermally controlled glacier surging. *Journal of Glaciology*, *47*(159), 527–538.
Gimbert, F., Tsai, V. C., Amundson, J. M., Bartholomaus, T. C., & Walter, J. I. (2016). Subseasonal changes observed in subglacial channel pressure, size, and sediment transport. *Geophysical Research Letters*, *43*, 3786–3794. https://doi.org/10.1002/2016GL068337
Harper, J. T., Bradford, J. H., Humphrey, N. F., & Meierbachtol, T. W. (2010). Vertical extension of the subglacial drainage system into basal crevasses. *Nature*, *467*(7315), 579–582.
Harrison, W. D., Echelmeyer, K. A., Chacho, E. F., Raymond, C. F., & Benedict, R. J. (1994). The 1987–88 surge of West Fork Glacier, Susitna Basin, Alaska, U.S.A. *Journal of Glaciology*, *40*(135), 241–254.
Harrison, W. D., & Post, A. S. (2003). How much do we really know about glacier surging? *Annals of glaciology*, *36*, 1–6.
Herzfeld, U. C., McDonald, B., Stachura, M., Hale, R. G., Chen, P., & Trantow, T. (2013). Bering Glacier surge 2011: Analysis of laser altimeter data. *Annals of Glaciology*, *54*(63), 158–170.
Kamb, B. (1987). Glacier surge mechanism based on linked cavity configuration of the basal water conduit system. *Journal of Geophysical Research*, *92*(B9), 9083.
Kamb, B., Raymond, C., Harrison, W., Engelhardt, H., Echelmeyer, K., Humphrey, N., et al. (1985). Glacier surge mechanism: 1982–1983 surge of Variegated Glacier, Alaska. *Science*, *227*(4686), 469–479.
King, E. C., Hindmarsh, R. C. A., & Stokes, C. R. (2009). Formation of mega-scale glacial lineations observed beneath a West Antarctic ice stream. *Nature Geoscience*, *2*(8), 585–588.
Kingslake, J., & Ng, F. (2013). Modelling the coupling of flood discharge with glacier flow during jökulhlaups. *Annals of Glaciology*, *54*(63), 25–31.
Lingle, C. S., & Fatland, D. R. (2003). Does englacial water storage drive temperate glacier surges? *Annals of Glaciology*, *36*, 14–20.
Lliboutry, L. (1968). General theory of subglacial cavitation and sliding of temperate glaciers. *Journal of Glaciology*, *7*(49), 21–58.
Lovell, H., Fleming, E. J., Benn, D. I., Hubbard, B., Lukas, S., Rea, B. R., et al. (2015). Debris entrainment and landform genesis during tidewater glacier surges. *Journal of Geophysical Research: Earth Surface*, *120*, 1574–1595. https://doi.org/10.1002/2015JF003509
Meier, M. F., & Post, A. (1969). What are glacier surges? *Canadian Journal of Earth Sciences*, *6*(4), 807–817.
Molnia, B. F., & Post, A. (2010). *Surges of the Bering Glacier*, (Vol. 462, pp. 291–316).
Mordret, A., Mikesell, T. D., Harig, C., Lipovsky, B. P., & Prieto, G. A. (2016). Monitoring southwest Greenland's ice sheet melt with ambient seismic noise. *Science advances*, *2*(5).
Murray, T., Strozzi, T., Luckman, A., Jiskoot, H., & Christakos, P. (2003). Is there a single surge mechanism? Contrasts in dynamics between glacier surges in Svalbard and other regions. *Journal of Geophysical Research*, *108*(B5), 2237. https://doi.org/10.1029/2002JB001906
Murray, T., Stuart, G. W., Miller, P. J., Woodward, J., Smith, A. M., Porter, P. R., & Jiskoot, H. (2000). Glacier surge propagation by thermal evolution at the bed. *Journal of Geophysical Research*, *105*(B6), 13,491–13,507.
Ng, F. S. (2000). Canals under sediment-based ice sheets. *Annals of Glaciology*, *30*, 146–152.
Obermann, A., Planès, T., Larose, E., Sens-Schönfelder, C., & Campillo, M. (2013). Depth sensitivity of seismic coda waves to velocity perturbations in an elastic heterogeneous medium. *Geophysical Journal International*, *194*(1), 372–382.
Pritchard, H. (2005). Glacier surge dynamics of Sortebræ, east Greenland, from synthetic aperture radar feature tracking. *Journal of Geophysical Research*, *110*, F03005. https://doi.org/10.1029/2004JF000233
Raymond, C. F. (1987). How do glaciers surge? A review. *Journal of Geophysical Research*, *92*(B9), 9121–9134.
Savage, M. K. (1999). Seismic anisotropy and mantle deformation: What have we learned from shear wave splitting? *Reviews of Geophysics*, *37*(1), 65–106.
Schoof, C. (2010). Ice-sheet acceleration driven by melt supply variability. *Nature*, *468*(7325), 803–806.
Schoof, C., & Hewitt, I. (2013). Ice-sheet dynamics. *Annual Review of Fluid Mechanics*, *45*(1), 217–239.
Schoof, C., Rada, C. A., Wilson, N. J., Flowers, G. E., & Haseloff, M. (2014). Oscillatory subglacial drainage in the absence of surface melt. *The Cryosphere*, *8*(3), 959–976.
Sevestre, H., Benn, D. I., Hulton, N. R. J., & Baelum, K. (2015). Thermal structure of Svalbard glaciers and implications for thermal switch models of glacier surging. *Journal of Geophysical Research: Earth Surface*, *120*, 2220–2236.

Sharp, M. (1985). "Crevasse-fill" ridges—A landform type characteristic of surging glaciers? *Geografiska Annaler: Series A, Physical Geography*, *67*(3-4), 213–220.
Toyokuni, G., Takenaka, H., Takagi, R., Kanao, M., Tsuboi, S., Tono, Y., et al. (2018). Changes in Greenland ice bed conditions inferred from seismology. *Physics of the Earth and Planetary Interiors*, *277*, 81–98.
Turrin, J., Forster, R. R., Larsen, C., & Sauber, J. (2013). The propagation of a surge front on Bering Glacier, Alaska, 2001–2011. *Annals of Glaciology*, *54*(63), 221–228.
Vivian, R. (1980). The nature of the ice-rock interface: The results of investigation on 20000 m^2 of the rock bed of temperate glaciers. *Journal of Glaciology*, *25*(92), 267–277.
Walder, J. S., & Fowler, A. (1994). Channelized subglacial drainage over a deformable bed. *Journal of Glaciology*, *40*(134), 3–15.
Walter, F., Dreger, D. S., Clinton, J. F., Deichmann, N., & Funk, M. (2010). Evidence for near-horizontal tensile faulting at the base of Gornergletscher, a Swiss alpine glacier. *Bulletin of the Seismological Society of America*, *100*(2), 458–472.
Walter, F., Roux, P., Roeoesli, C., Lecointre, A., Kilb, D., & Roux, P.-F. (2015). Using glacier seismicity for phase velocity measurements and Green's function retrieval. *Geophysical Journal International*, *201*(3), 1722–1737.
Weertman, J. (1972). General theory of water flow at the base of a glacier or ice sheet. *Reviews of Geophysics*, *10*(1), 287–333.
Worthington, L. L., Van Avendonk, H. J. A., Gulick, S. P. S., Christeson, G. L., & Pavlis, T. L. (2012). Crustal structure of the Yakutat terrane and the evolution of subduction and collision in southern Alaska. *Journal of Geophysical Research*, *117*, B01102. https://doi.org/10.1029/2011JB008493
Zhan, Z., Tsai, V. C., & Clayton, R. W. (2013). Spurious velocity changes caused by temporal variations in ambient noise frequency content. *Geophysical Journal International*, *194*(3), 1574–1581. https://doi.org/10.1093/gji/ggt170